Search and analysis of giant radio galaxies with associated nuclei (SAGAN). II. Molecular gas content of giant radio galaxies

P. Dabhade, F. Combes, P. Salomé, J. Bagchi, M. Mahato

Astronomy
&
Astrophysics

Search and analysis of giant radio galaxies with associated nuclei (SAGAN)

II. Molecular gas content of giant radio galaxies[*]

P. Dabhade[1,2], F. Combes[3,4], P. Salomé[3], J. Bagchi[2], and M. Mahato[2]

[1] Leiden Observatory, Leiden University, PO Box 9513, 2300 RA Leiden, The Netherlands
   e-mail: `pratik@strw.leidenuniv.nl`
[2] Inter-University Centre for Astronomy and Astrophysics (IUCAA), Pune 411007, India
[3] Sorbonne Université, Observatoire de Paris, Université PSL, CNRS, LERMA, 75014 Paris, France
[4] Collège de France, 11 Place Marcelin Berthelot, 75231 Paris, France

ABSTRACT

Radio galaxies with jets of relativistic particles are usually hosted by massive elliptical galaxies with active nuclei powered by accretion of interstellar matter onto a supermassive black hole. In some rare cases (<5%), their jets drive the overall structure to sizes larger than 700 kpc, and they are called giant radio galaxies (GRGs). A very small fraction of the population of such radio galaxies contains molecular and atomic gas in the form of rings or discs that can fuel star formation. The origin of this gas is not well known; it has sometimes been associated with a minor merger with a gas-rich disc galaxy (e.g. Centaurus A) or cooling of material from a hot X-ray atmosphere (e.g. cooling flows). The giant radio jets might be the extreme evolution of these objects, and they can teach us about the radio galaxy evolution. We selected 12 targets from a catalogue of 820 GRGs that are likely to be in a gas-accretion and star formation phase. The targets were selected from the mid-infrared to contain heated dust. We report here the results of IRAM-30m observations, the molecular gas content, and the star formation efficiency, and we discuss the origin of the gas and disc morphology. Three out of our 12 targets are detected, and for the others, we report significant upper limits. We combine our three detections and upper limits with four additional detected GRGs from the literature to discuss the results. Most of the GRG targets belong to the main sequence, and a large fraction are in the passive domain. Their star formation efficiency is comparable to normal galaxies, except for two galaxies that are deficient in molecular gas with a short (∼200 Myr) depletion time, and a quiescent gas-rich giant spiral galaxy. In general, the depletion time is much longer than the lifetime of the giant radio jet.

Key words. galaxies: active – galaxies: ISM – galaxies: jets – galaxies: nuclei – galaxies: spiral – radio continuum: galaxies

1. Introduction

It has recently become evident that galaxies and their central supermassive black holes (SMBHs) co-evolve (Heckman & Best 2014), and new research continues to bring forth new facts that improve our understanding. The simultaneous growth of SMBHs and bulges of galaxies might be a consequence of AGN feedback, which plays a fundamental regulating role on star formation (SF), and might result in the observed tight correlation between their masses (e.g. Croton et al. 2006; Magorrian et al. 1998; Marconi & Hunt 2003). Energy transfer from the AGN can produce outflows and temporarily starve galaxies of fresh gas, thus quenching the star formation (e.g. Cicone et al. 2014). It is now understood that the galaxy's SMBH can play a vital role in its growth and evolution, and vice versa. The most spectacular manifestations of massive black holes in AGNs are the powerful bipolar relativistic jets that produce twin-lobed structures on ∼10^2–10^3 kpc scales. Most of the time, evidence for SF quenching is obtained from studying radio-loud AGN, where molecular gas is entrained by the radio jets. These radio galaxies (RGs) are a unique opportunity to study the AGN-fueling process during the radio-mode phase as well as the AGN feedback.

The AGN feedback and outflows can be studied through the cold molecular gas properties of the galaxy, and current stud-ies have been restricted to mostly luminous AGNs. In the past three decades, several studies at lower (Evans et al. 2005; Ocaña Flaquer et al. 2010; Prandoni et al. 2010; Smolčić & Riechers 2011; Salomé et al. 2015; Lanz et al. 2016; Ruffa et al. 2019) and higher redshifts (Hughes et al. 1997; van Ojik et al. 1997; De Breuck et al. 2003; Emonts et al. 2014; Nesvadba et al. 2017) have been conducted to probe the molecular gas content, SFR, and cold gas as potential fuel supply in RGs. A CO study of a sample of low-luminosity RGs carried out by Prandoni et al. (2010) supported the idea that RGs might be fuelled by cold gas, restricted to kiloparsec-scale nuclear discs or rings around the AGN. Ruffa et al. (2019) have shown a strong possibility that jet-cold gas interacts in a few objects. They also reported inflows inferred from dominant radial motions, indicating that cold gas fuels the RGs.

The members of an extreme sub-class of RGs, which grow to megaparsec scales and are relatively rare, are called the Giant Radio Galaxies (GRGs). The projected linear size of GRGs is greater than 0.7 Mpc and can grow to about 5 Mpc, which is comparable to large galaxy clusters. This makes them one of the largest single astrophysical objects known to date. They have accreting SMBHs of mass 10^8–10^{10} $M_\odot$, which under certain conditions launch collimated bipolar relativistic jets orthogonal to their accretion disc (Lynden-Bell 1969; Begelman et al. 1979). Like normal radio galaxies, GRGs are almost always hosted by

---

[*] Based on observations carried out with IRAM-30m.

bright elliptical galaxies. GRGs were discovered (Willis et al. 1974) almost 20 years after the discovery of RGs (Jennison & Das Gupta 1953), and since then, only about 820 (Dabhade et al. 2020a) of them have been found, compared to thousands of RGs.

Some CO observations of GRGs have been attempted before (3C236: Labiano et al. 2013, 3C 326: Nesvadba et al. 2010) but were mostly single-object studies. Saripalli & Mack (2007), as part of their work on restarted RGs, observed five GRGs with the 15m Swedish-ESO Millimetre Telescope (SEST) in the CO(1-0) and CO(2-1) line transitions and obtained only upper limits for all their GRGs.

To understand these extreme cosmic radio sources better, and specifically, to address the key questions about their size and power, we have initiated a project called Search and Analysis of GRGs with Associated Nuclei (SAGAN[1]), whose pilot study was presented in Dabhade et al. (2017). In this project, we have built an uniform database of all known GRGs, which was lacking before (Dabhade et al. 2020a). With this GRG database, we aim to carry out multi-wavelength studies of their host galaxies, focusing on physical properties such as their black hole accretion rate; the excitation type, which is either high-power radiatively efficient giant radio galaxies ("high-excitation", HEGRGs) or low-power radiatively inefficient giant radio galaxies ("low-excitation", LEGRGs); the black hole mass (M_{BH}); their galaxy star formation rate (SFR); and their molecular gas content. The key to understanding the giant nature of GRGs may lie in the accretion properties of these peculiar AGNs, and we can probe this by tracing molecular gas to determine whether these objects are fueled by cold gas in the disc. The presence or absence of cold molecular gas in the host galaxies of GRGs can provide information about their star formation rate, accretion state, and stellar mass properties.

This paper is organised in the following way: in Sect. 2 we describe our sample, observations are presented in Sect. 3, and the results are reported in Sect. 4. The interpretation of these results is presented and their effect on the evolution scenarios is discussed in Sect. 5. The conclusions of our work are presented in Sect. 6. To compute distances, we have adopted a flat ΛCDM cosmology, with $\Omega_m = 0.29$, $\Omega_\Lambda = 0.71$, and the Hubble constant of $H_0 = 70 \, \text{km s}^{-1} \, \text{Mpc}^{-1}$.

2. The sample

With the project SAGAN (Dabhade et al. 2020a), we have created the largest database of GRGs to date, and we applied the following criteria to form a sub-sample to be studied at millimetre waves using IRAM-30m (Baars et al. 1987) to probe the cold molecular gas content: (i) the GRG is not hosted by a quasar, (ii) the GRG is well detected in the Wide-field Infrared Survey Explorer (WISE) at $22 \, \mu\text{m}$ (fourth band) (Wright et al. 2010), (iii) the redshift of the host galaxy of the GRG is accurately known from spectroscopic measurements, and (iv) the GRG is observable in the sky of IRAM-30m telescope. GRGs, like RGs, are mainly early-type galaxies, and only a minority of them (~17%, Kozieł-Wierzbowska et al. 2020) are late types and may still have some gas; the WISE selection is there to find this minority. After applying all the above filters to our GRG-catalogue, we selected a sample of 12 GRGs that is representative of this minority; the GRGs are listed in Table 1. In Cols. 3 and 4 of Table 1 we list the accurate position (RA and Dec) of the

host galaxies, and their accurate spectroscopic redshifts are listed in Col. 5. Column 6 includes the luminosity distances of the sources. The information obtained from the WISE fourth band and its derived properties are presented in Cols. 7 and 8, where in Col. 8, $L_{22\,\mu\text{m}}$ is the luminosity of the host galaxies at $22\,\mu\text{m}$. Column 9 contains the GRG references of the sources and/or the optical identification. Figure 1 displays the SDSS images for the sources when they are available. For the others, the PanSTARRS i band images of the hosts of the GRGs in our sample are given in Fig. 2.

For all the 12 galaxies of the sample, the star formation rate (SFR) was first estimated from the $22\,\mu\text{m}$ luminosity (Calzetti et al. 2007). When a more accurate estimate existed in the literature from the SED or multi-wavelength tracers, we used it from Chang et al. (2015) for R1-2, R1-3, R2-0, R2-3, R2-6 to R2-9, and from Salim et al. (2018) for R2-0, R2-3, R2-7 and R2-8. Because several estimates are available, we took an average value. SFR tracers in general suffer from uncertainties, but the SFR estimated from $22\,\mu\text{m}$ was found to be compatible within the uncertainties with the value derived from the FIR when available. Moreover, recent studies of Cluver et al. (2014), Gürkan et al. (2015), and Catalán-Torrecilla et al. (2015) have used $22\,\mu\text{m}$ from WISE to determine the SFR effectively. Although the $22\,\mu\text{m}$ flux could also come from the AGN, it is statistically well correlated to the more specific far-infrared SFR indicator, even for AGN (Gürkan et al. 2015). Stellar masses were estimated from observed optical and near-infrared (NIR) magnitudes, using standard relations as a function of colours, derived from stellar population models (Bell et al. 2003). Because the targets have a low redshift, K-corrections were applied using the analytical approximations from Chilingarian et al. (2010). All adopted values are listed in Table 2, together with the CO results we obtained using IRAM-30m data. Table 2 also lists the angular sizes (Col. 2) of the galaxies, acquired by us from the i-band stellar profiles of the galaxies: ten were from the SDSS, and four from PanSTARRS, see Figs. 1 and 2.

2.1. R1-1: 2MASX J23453268−0449256

The galaxy 2MASX J23453268−0449256 (R1-1) is one of the largest (projected linear size ~1.6 Mpc at radio wavelengths) radio galaxy known to date, hosted by a massive, late-type spiral galaxy that lacks a classical bulge at the redshift of 0.0755 (Bagchi et al. 2014). It shows FR-II and double-double (two sets of lobes, indicating episodic activity) radio morphology; the jet axis is nearly orthogonal to the disc of the host galaxy. This is very unusual because such large-scale radio jets are in general hosted by ellipticals (Taylor et al. 1996; McLure et al. 2004). It shows several other unusual properties that challenge the standard paradigms for black hole growth in galaxies lacking classical bulges. Its general properties as presented by Bagchi et al. (2014, and in prep.) are similar to those of passive red spirals (Masters et al. 2010), although the WISE mid-infrared (mid-IR) colours suggest that star formation is still occurring within its disc. With $M_r \sim -23.0$ mag, it lies at the very top of the luminosity function of red spirals. The galaxy rotation curve derived from the Hα line peaks at about $429 \pm 30 \, \text{km,s}^{-1}$ at a large radius, which is quite high for spirals, after correcting for $i = 65°$ inclination angle (cf. HyperLeda[2]). This implies an estimated dynamical mass of $\sim 10^{13} \, M_\odot$ within the virial radius of 450 kpc, assuming a flat rotation curve. The central bulge velocity dispersion is $\sigma = 351 \pm 25 \, \text{km s}^{-1}$, which is close to the highest velocity

Table 1. General properties of our sample of 12 GRGs.

Sr. No	Name	RA (HMS)	Dec (DMS)	z	D_L (Mpc)	W4 (22 μm) mag (snr)	Log $L_{22\,\mu m}$ (erg s^{-1})	Refs.
(1)	(2)	(3)	(4)	(5)	(6)	(7)	(8)	(9)
R1-1	2MASX J23453268−0449256	23 45 32.70	−04 49 25.4	0.07557	342	7.135 (8.5)	43.35	(1)
R1-2	CGCG 245−031	13 12 17.00	+44 50 21.3	0.03557$^{(\dagger)}$	156	8.133 (5.7)	42.27	(2)
R1-3	B2 1029+28	10 32 14.02	+27 56 01.7	0.08519$^{(\dagger)}$	389	6.821 (11)	43.58	(2)
R2-1	WNB0313+683	03 18 18.98	+68 29 31.4	0.09010	412	6.187 (23.9)	43.18	(3)
R2-2	LCRS B132559.3−025215	13 28 34.37	−03 07 44.8	0.08526$^{(\dagger)}$	389	7.067 (13.5)	42.77	(4)
R2-3	2MASX J14504940+1006497	14 50 49.40	+10 06 49.1	0.05453$^{(\dagger)}$	243	8.112 (4.9)	41.95	(5)
R2-4	NGC 6251	16 32 31.97	+82 32 16.4	0.02471	108	5.561 (33)	42.24	(6)
R2-5	LEDA 2785926	21 45 30.90	+81 54 53.7	0.14570	692	6.320 (28.3)	43.57	(7)
R2-6	B2 0951+27	09 54 19.19	+27 15 59.9	0.47120$^{(\dagger)}$	2649	7.469 (7.0)	44.26	(8,9)
R2-7	LEDA 1406818	10 21 24.21	+12 17 05.4	0.12940$^{(\dagger)}$	606	8.248 (3.5)	42.66	(10)
R2-8	Speca	14 09 48.85	−03 02 32.5	0.13749$^{(\dagger)}$	651	8.332 (2.2)	42.69	(11)
R2-9	J121615.21+162432.1	12 16 15.21	+16 24 32.2	0.45908$^{(\dagger)}$	2569	7.556 (6.3)	44.19	(12)
R1-0	PKS 0211−031	02 13 47.00	−02 56 37.5	0.35679	1906	7.412 (8.8)	44.73	(13)
R2-0	B2 0915+32B (NE)	09 18 59.41	+31 51 40.7	0.06212	278	8.582 (3.3)	41.85	(14)

Notes. Here R1 and R2 refer to observation runs 1 and 2 with IRAM-30m. RA and Dec are expressed in the J2000 coordinate system. Object R1-0 is a radio-loud quasar, and object R2-0 is a radio galaxy. These two objects were recently classified as non-GRGs based on new available data. All the redshifts listed in Col. 5 are from spectroscopic measurements, where redshifts marked with a dagger are taken from the SDSS. In the absence of SDSS spectroscopic redshift measurement, the redshift was taken from the reporting paper (Col. 9). Columns 7 and 8 represent the WISE band 4 magnitude and luminosity, respectively.

References. (1) Bagchi et al. (2014); (2) Schoenmakers et al. (2001); (3) Schoenmakers et al. (1998); (4) Machalski et al. (2001); (5) Clarke et al. (2017); (6) Waggett et al. (1977); (7) Schoenmakers et al. (2000); (8) Proctor (2016); (9) Amirkhanyan (2016); (10) Kozieł-Wierzbowska & Stasińska (2011); (11) Hota et al. (2011); (12) Dabhade et al. (2020a); (13) Owen et al. (1995); (14) Kuźmicz et al. (2018).
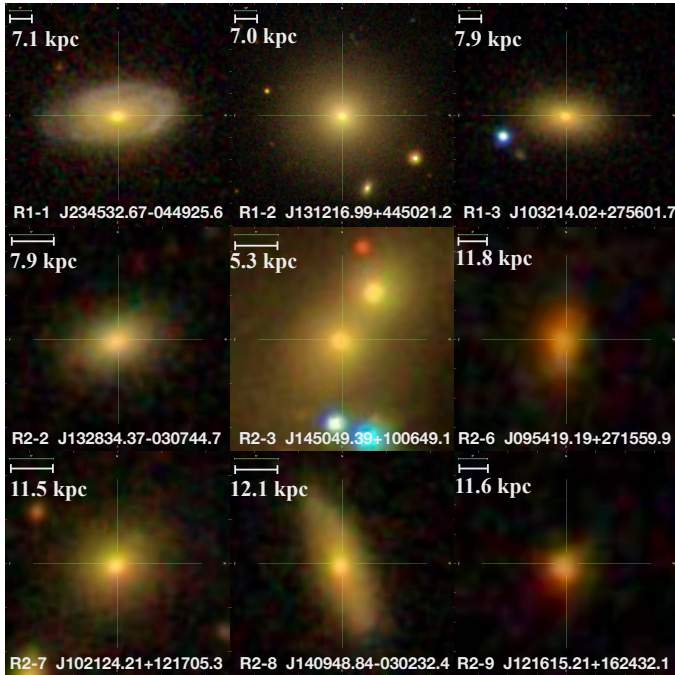

Fig. 1. Host galaxies of nine GRGs from SDSS. The bar at the top left represents the angular scale in kpc for reference.

Fig. 2. PanSTARRS *i*-band image of the hosts of GRGs that are absent in the SDSS footprint. The bar at the bottom indicates the angular scale of 5″, 20″, and 10″ in kiloparsec (kpc) for R2-1, R2-4, and R2-5, respectively.

is highly elongated parallel to the host galaxy disc, suggesting that feedback by the radio jet has disrupted or expelled hot gas from a region extending roughly 80 kpc above and below the disc plane. Radio-mode feedback like this is rarely seen in spiral galaxies (Mukherjee et al. 2016, 2018).

2.2. R1-2: CGCG 245−031

CGCG 245−031 (R1-2) is a flat-spectrum radio source (Healey et al. 2007). It has a low value for its integrated spectral index and is a young radio source. It is a good candidate for a restarting class.

2.3. R1-3: B2 1029+28

B2 1029+28 is hosted by a Seyfert type-1 galaxy (Véron-Cetty & Véron 2006) called 2MASX J10321402 + 2756015. In this galaxy, the stellar populations are not old, but have intermediate ages (Kuźmicz et al. 2019).

dispersion found among nearby E and S0 galaxies (van den Bosch et al. 2012). Walker et al. (2015) used *Chandra* to detect the hot X-ray halo of the galaxy, which extends to $r > 80$ kpc; it is one of just a few high-mass spirals for which hot gaseous haloes have directly been detected through X-ray imaging to date (Bregman et al. 2018). Intriguingly, the X-ray emitting hot halo
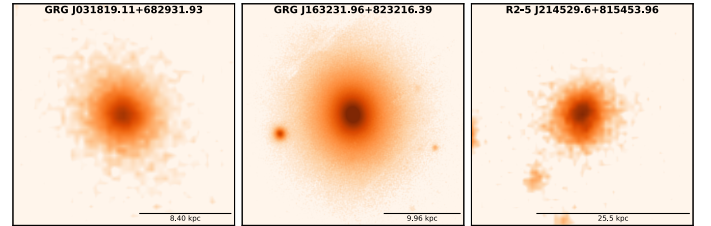
Table 2. Derived properties of the GRG sample.

Sr. No	R_e (arcsec)	R_e (kpc)	SFR ($M_\odot$ yr^{-1})	CO(1-0) (Jy km s^{-1})	CO(2-1) (Jy km s^{-1})	$\log M(H_2)$ ($M_\odot$)	$t_{\rm dep}$ Gyr	$\log M_*$ ($M_\odot$)
(1)	(2)	(3)	(4)	(5)	(6)	(7)	(8)	(9)
R1-1	5.4	7.76	2.95	14.0	16.3	10.21	5.49	11.37
R1-2	6.1	4.32	0.19	<1.7	<2.7	<8.63	<2.24	10.51
R1-3	3.6	5.77	2.45	<1.5	<7.5	<9.35	<0.91	10.84
R2-1	0.96	1.62	2.07	<1.3	<2.2	<9.34	<1.05	10.63
R2-2	2.2	3.53	0.91	<0.9	<1.3	<9.13	<1.48	10.52
R2-3	0.78	0.83	0.09	<0.9	<1.9	<8.73	<5.96	11.25
R2-4$^{(2)}$	15.6	7.78	0.31	<1.2	<4	<8.16	<0.47	11.40
R2-5	0.7	1.79	4.64	<1.1	<1.9	<9.69	<1.06	11.03
R2-6$^{(1)}$	0.95	5.63	170	<1.3	<2.7	<10.82	<0.39	11.70
R2-7	2.4	5.59	1.44	<1.1	<1.9	<9.59	<2.70	11.41
R2-8	3.3	8.04	1.48	<0.9	1.1	9.04	0.74	11.50
R2-9$^{(1)}$	0.6	3.55	8.33	0.54	<1.1	10.42	3.15	10.89
R1-0$^{(1)}$	0.87	4.37	48.9	<0.45	<1.6	<10.11	<0.26	10.87
R2-0	5.6	6.70	0.47	<1.1	<2.7	<8.93	<1.81	11.46

Notes. R_e is the half-light radius, SFR is the star formation rate, CO refers to CO flux in the respective bands, $\log M(H_2)$ represents the molecular mass (log scale), $t_{\rm dep}$ is the depletion time, and $\log M_*$ refers to the stellar mass (log scale) of the galaxy. $^{(1)}$ For these sources, we observed CO(3-2) instead of CO(2-1). $^{(2)}$ This source was also observed by Ocaña Flaquer et al. (2010). All upper limits are computed at 3σ and assuming an $FWHM = 300$ km s^{-1}.

2.4. R2-1: WNB0313+683

The GRG R2-1 or WNB0313+683 has a projected linear size of 1.52 Mpc with a GHz-peaked spectrum (GPS) core, FR-II type morphology, and recurrent activity (Schoenmakers et al. 1998; Bruni et al. 2019). It is hosted by a Seyfert type-1 galaxy (LEDA 3095635) at $z \sim 0.09$ that is detected in hard X-rays (Winter et al. 2008). Schoenmakers et al. (1998) estimated its spectral age to be ~144 Myr, but recently, Machalski (2011) estimated the age of the lobes to be ~250 Myr.

2.5. R2-2: LCRS B132559.3−025215

Machalski & Condon (1999) identified LCRS B132559.3−025215 as a GRG. It is hosted by the Seyfert 2-type (Véron-Cetty & Véron 2006) galaxy called 2MASX J13283434−0307442.

2.6. R2-3: 2MASX J14504940+1006497

Source R2-3 is hosted by a central dominant galaxy (the core of a triplet, which is also known as UGC 09555 NED03) of a low-density galaxy group (MSPM 02158), as shown in Fig. 1. Based on their SED analysis, Clarke et al. (2017) concluded that the host galaxy is an S0-type galaxy with an SFR of $1.2 \pm 0.3\,M_\odot$ yr^{-1}. Clarke et al. (2017) also presented its LOFAR 142 MHz radio map, which reveals a large diffuse structure that is not seen in any other radio survey. The bright radio core and high diffuse emission along the jet axis strongly indicate a restarted source. Based on its radio core spectrum, it has been classified as a flat-spectrum galaxy (Healey et al. 2007) with frequencies between ~1 to 10 GHz, and it has an inverted core spectrum with frequencies between 22 to 43 GHz (Park et al. 2013). This further supports the hypothesis that this is a restarted AGN.

2.7. R2-4: NGC 6251

NGC 6251 is our nearest target, and it has been the object of many observations since its identification (Waggett et al. 1977; Laing et al. 1983). Chen et al. (2011) studied the neighbouring 17 galaxies, which may form a loose group, but with very low background X-ray gas, explaining the large 1.6 Mpc radio jets. The main jet and lobes are centre-brightened like FR-I, but there are also hot spots near the end of the north and south lobes that suggest a FR-II type of morphology. The radio power is in between the two FR types. Recent LOFAR observations at 150 MHz have revealed low surface brightness extensions and backflows of the lobes (Cantwell et al. 2020), with ages older than 200 Myr. A dust lane has been discovered by Nieto et al. (1983), roughly parallel to the radio jet, with a size of about 5 kpc. The inner orientation of the jets is still unclear; it appears at least that the inner jet and outer lobes are misaligned (Jones & Wehrle 2002).

2.8. R2-8: Speca

Only about ten RGs (Ledlow et al. 2001; Hota et al. 2011; Bagchi et al. 2014; Singh et al. 2015; Mao et al. 2015; Mulcahy et al. 2016) have been found to be hosted by spiral galaxies up to now, and only two (2MASX J23453268−0449256 and Speca) of them belong to the GRG subclass. Along with its unusual property of being hosted by a spiral (Hota et al. 2011), Speca is classified as the central galaxy, called MaxBCG J212.45357-03.04237 cluster or group. Another peculiar property of this object is its three pairs of lobes, also called a triple-double, with clear evidence of restarting activity. The outer lobes look like relics revived by shocks coming from the interaction between the cluster and cosmic filaments. The galaxy shows very recent star formation that might be fueled by a cooling flow from merging activity ~500 Myr ago (Hota et al. 2011).

2.9. Other GRGs

R2-5 (Seyfert 2) and R2-7 are also dominant galaxies of their groups, with indications of star formation in the recent past (Kuźmicz et al. 2019). R2-9 is one of the most recently identified GRG, at relatively high redshift (Dabhade et al. 2020a). It appears to be actively forming stars. R2-9 is the most luminous GRGs at 22 microns (WISE band 4) in our sample, and appears to be harbouring a dust-obscured powerful AGN based on its red colour.

2.10. Non-GRGs

At the beginning of our study, two objects were thought to be GRG and were observed at IRAM. We report the results, which may serve other studies, although the objects are not GRGs, but normal RGs or RQs. B2 0915+32B is a galaxy pair, and the two companions lie at a distance of 43 kpc. The early-type northern galaxy is the host of the giant radio jet, and its southern companion is a late-type blue spiral galaxy, which could be the reservoir of gas to fuel the northern AGN. PKS 0211-031 is radio-loud quasar with FR-II type morphology.

3. Observations

Observations of the CO(1-0), CO(2-1) (and for one target CO(3-2)) emission lines have been carried out with the IRAM-30m telescope at Pico Veleta, Granada, Spain, during June and September 2016 for the first run (called R1), and then in March 2020 for the second run (called R2). The beam full width at half-maximum (FWHM) is 23″ and 12″ at the frequencies of 115 GHz and 230 GHz, respectively. The redshifts of our targets (except for two objects) range from 0 to 0.1, and the corresponding beams are up to 10% larger, accordingly. The SIS receivers (EMIR) were used for observations in the wobbler-switching mode, and the reference positions were offset by ± 120 arcsec in azimuth. The main-beam efficiency of IRAM is $\eta_{mb} = T_A^*/T_{mb} = 0.79$ and 0.63 at 105 GHz and 210 GHz, respectively. The system temperatures ranged between 150 K and 400 K at 2.6 mm, and between 200 K and 600 K at 1.3 mm. The pointing was regularly checked every two hours on a nearby planet or a bright continuum source, and the focus was reviewed after each sunrise or when a suitable planet was available, as well as at the beginning of each day. The time on source typically ranged from four to five hours, depending on the weather. Two backends were used simultaneously, the Wideband Line Multiple Autocorrelator (WILMA) and the Fourier transform spectrometer (FTS). The T_{mb} rms noise level in four hours of integration was $\sigma_{mb} \sim 0.7$ mK with a spectrometer resolution of 50 km s^{-1} for 105 GHz and $\sigma_{mb} \sim 0.9$ mK for 210 GHz. These can be lower in very good weather. The upper limits reported in the next section for the integrated CO fluxes are computed by S(CO)dV $= 3 \times$ rms$_{300}$ JypK $\times 300$ km s^{-1}, where JypK is the conversion from K to Jy ($=5$ Jy K^{-1} for the IRAM-30m), and rm$_{300}$ is the rms estimated in 300 km s^{-1} wide bins. A typical FWHM of 300 km s^{-1} is usually taken for early-type galaxies, which RGs and GRGs are, as reported in the catalogue by Young et al. (2011).

Two of our sample sources have previously been observed with the IRAM-30m by Ocaña Flaquer et al. (2010). For NGC 6251, we combined our spectra in CO(1-0) to improve the upper limit and provide a CO(2-1) search, which was lacking. As for B2 0951+32B, which is a pair of galaxies with a projected separation of 36″, the previous pointing was directed towards the

NED middle position in between the two galaxies, and did not cover either. We observed towards the north-eastern elliptical galaxy, which is the host of the RG (Fanti et al. 1987).

4. Results

As shown in Table 2, only the spiral galaxy R1-1 (J2345−0449) has been clearly detected, and upper limits are reported for the 11 other GRGs, with tentative detections for 2 of them. The two-horn spectra of R1-1 (Fig. 3) were fitted by three Gaussians each, and the fits are reported in Table 3. These fits are only empirical, which is better for computing the total intensity, but do not imply any underlying physical components. The upper limit for the R1-0 RG (PKS0211−031) is relatively high because it is a source with one of the highest redshifts. However, the molecular mass is expected to increase with redshift (Tacconi et al. 2018), and based on the measured SFR, a much higher molecular mass was expected. Therefore the upper limit is significant. The tentative signals are displayed in Fig. 4 for CO(2-1) in the spiral galaxy Speca, and for CO(1-0) for J121615.21+162432.1. Only linear baselines were subtracted from the spectra, but uncertainties are still present because of the presence wavy baselines, although the signal appears at 5σ and 6σ, respectively.

In the following subsections, we present the results we derived from our detections and upper limits of the molecular gas content of the hosts of GRGs, and also compare it with the SFR derived from the mid-IR fluxes. All our upper limits are significant, as we discuss in Sect. 5 and show in particular in Figs. 8 and 9. In these scaling relations, the upper limits are within or below the expectations. Using our observed quantities, we were also able to estimate the gas depletion time $t_{dep} = M(H_2)/$SFR and compare it with the radiative lifetime of the GRGs. From the shape of the detected profile (two-horn shape, and contrast), we derived the gas concentration in the host and discuss the origin of the cool gas. The two-horn profile indicates an extended disc or ring, which is relaxed in the potential, suggesting a quite old galaxy accretion or merger origin for the gas. When the gas comes from cooling filaments alone, it generally has no time to relax in the galaxy potential, and no such profile is expected.

4.1. Molecular masses

To quantify the amount of molecular gas found in each target, we relied on the empirically established proportionality between the CO(1-0) luminosity and H$_2$ mass for a large number of Milky Way-like galaxies (e.g. Bolatto et al. 2013). We converted the integrated intensities in each beam (in T_{mb}) into integrated fluxes S(CO)dV, with a conversion of 5 Jy per Kelvin, as appropriate for the IRAM-30m telescope. From the integrated CO(1-0) flux S(CO)dV (Jy km s^{-1}) found within each region, the molecular mass was obtained through the formula (e.g. Solomon & Vanden Bout 2005)

$$L'_{CO}(K \, \text{km s}^{-1} \, \text{pc}^{-2}) = 3.25 \times 10^7 \frac{S(CO)dV}{(1+z)} \left(\frac{D_L}{\nu_{rest}}\right)^2, \quad (1)$$

where $\nu_{rest} = 115.271$ GHz, and D_L is the luminosity distance in megaparsec. The molecular mass, including helium, was then derived from $M(H_2) = 4.36 \, L'_{CO}$ assuming the standard CO-to-H$_2$ conversion factor of $X_{CO} = 2 \times 10^{20}$ cm^{-2}(K km s^{-1})$^{-1}$, as applicable to Milky Way-like galaxies. The region encompassed by the CO(1-0) beams in each galaxy is sufficiently large to cover the entire CO emission (even in the nearest galaxy, NGC 6251 (R2-4), it is 11 kpc). It is, therefore, possible to compare the
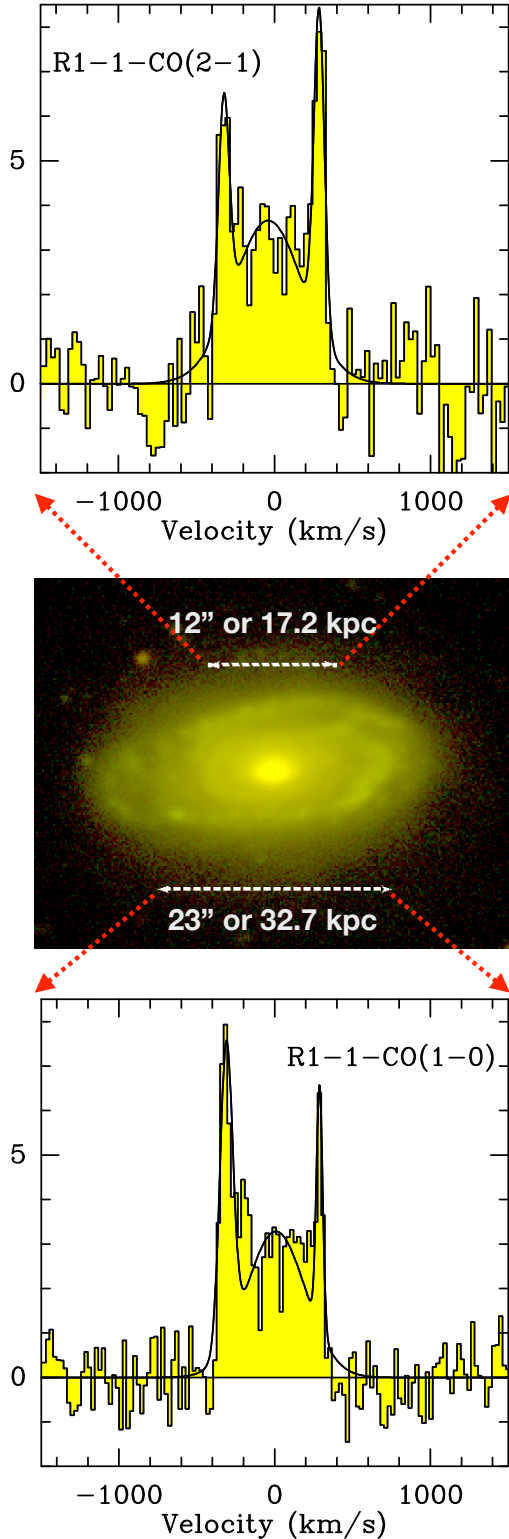
Fig. 3. Two spectra obtained towards R1-1 or GRG-J2345−0449 in CO(1-0) (*bottom*) and CO(2-1) (*top*). The vertical scale is T_{mb} in mK. The middle optical image of the host spiral galaxy of J2345−0449 is obtained by combining *G*- and *R*-band data of MegaCam on the CFHT. The *G*- and *R*-band data belong to the first-generation filters on the MegaCam. The scale on the image represents the beam of the IRAM observations at the respective frequencies.

total molecular masses with other published samples without any aperture correction.

Table 3. Fit results for R1-1 (GRG-J2345−0449) CO spectra.

Line	Area[1] mK km s^{-1}	V km s^{-1}	$FWHM$ km s^{-1}	T_{mb} Peak mK
CO(1-0)	1232 ± 167	-316 ± 4	207 ± 11	5.6 ± 0.8
CO(1-0)	800 ± 121	10 ± 18	235 ± 50	3.2 ± 0.8
CO(1-0)	779 ± 150	291 ± 15	179 ± 30	4.1 ± 0.8
CO(2-1)	930 ± 115	-324 ± 8	141 ± 20	6.2 ± 0.9
CO(2-1)	1368 ± 265	-35 ± 33	357 ± 70	3.6 ± 0.9
CO(2-1)	972 ± 110	286 ± 5	113 ± 13	8.1 ± 0.9

Notes. (1) Integrated signal in the main-beam temperature scale.

4.2. Deconvolving the two-horn spectra

In Fig. 3 the CO(1-0) and CO(2-1) spectra show a two-horn shape, with a different depth between the two peaks; the CO(1-0) spectrum is deeper. This means that the molecular component is not too highly concentrated towards the centre and that we are beginning to resolve it in the CO(2-1) line. Because the rotational velocity is zero at the nucleus, the central part of the profile is boosted by a high gas concentration. With a large beam, that is, for CO(1-0), the outer parts of the disc are preponderant, and the two-horn profile is more contrasted. The smaller CO(2-1) beam begins to resolve the disc, and the central part is more weighted than the outer parts in this line profile. To interpret the kinematics of our CO data more quantitatively, we used a simple analytical model that computes the velocity spectrum from the rotation velocity profile of the galaxy (Wiklind et al. 1997). The rotation velocity profile is determined from the stellar mass distribution, assuming it follows the simple potential-density pair proposed by Hernquist (1990). We adjusted the size and mass of the stellar component to fit the half-light radius and M_* as shown in Table 2. We completed this mass at high radii by dark matter, in order to flatten the rotation curve. The dark matter mass inside 24.5 kpc was taken to be $1.5 M_*$, and its characteristic radius was three times that of the stars. The gas disc was also taken into account in the potential, as shown in Fig. 5, with the mass shown in Table 2. Its characteristic scale can be determined by modelling the two-horn spectra. Based on the ellipticity obtained from the optical image (Fig. 1), we derive an inclination of 65°, which is also close to the value given by Hyperleda (65.7°).

The gas distribution is assumed to be axisymmetric with a surface density $\Sigma(r)$ in a disc with negligible thickness. For each velocity dv, the code calculates the density contained in the isovelocity (Eq. (2)). The velocity spectrum corresponds to the velocity histogram. We then convolved the computed spectrum with a Gaussian with a standard $\sigma = 10$ km s^{-1} to account for the gas velocity dispersion,

$$\frac{dN}{dv}(v) = \int \frac{\Sigma(r) \, r \, dr}{v_{rot}(r) \sin i \left(1 - \left[\frac{v}{v_{rot}(r) \sin i}\right]^2\right)^{1/2}}. \quad (2)$$

To determine the concentration of gas in the galaxy, we adopted an analytical profile, with a potential-density pair, which facilitates computing the rotation velocity. We selected the formulation of a Toomre disc of order 2: $\Sigma(r) = \Sigma_0 \left(1 + \frac{r^2}{d^2}\right)^{-5/2}$ (Toomre 1964). Figure 5 shows that the profile is close to an exponential, which is realistic. We also tried models with rings, using the difference between two Toomre discs with different scales, but a single gas disc was an even better fit. The exponential scale of the
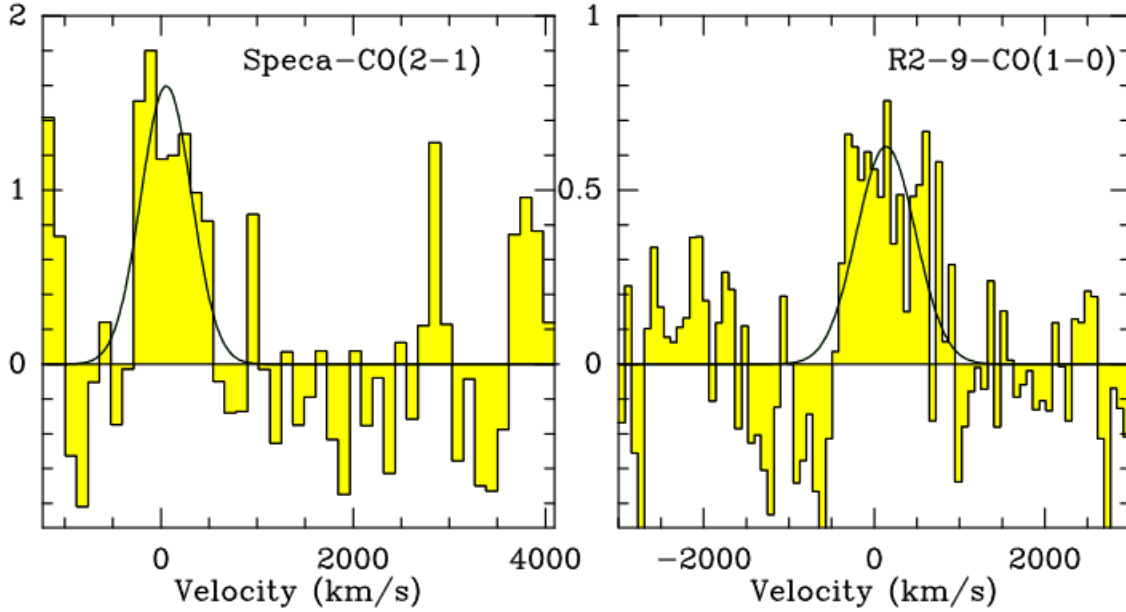
Fig. 4. Tentative spectra obtained towards Speca in CO(2-1) (*left*) and R2-9 in CO(1-0) (*right*). The vertical scale is T_{mb} in mK. The CO(2-1)/CO(1-0) line ratios for the two objects are within reasonable expectations, as shown in Table 2.
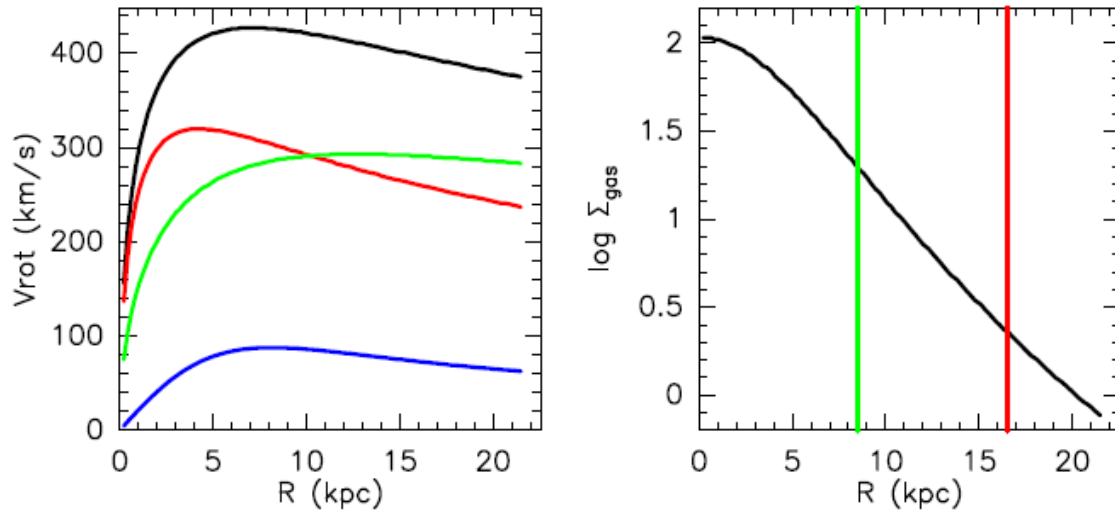

Fig. 5. Mass model for R1-1 or GRG-J2345−0449 (*left*), with the contributions to the rotational velocity of the stellar mass (red), the dark matter (green), and the gas (blue). The *right panel* shows the adopted gas surface density. The two vertical lines indicate the FWHM beam of the CO(1-0) (red) and CO(2-1) (green).

best-fit disc is 4.34 kpc, leading to a half-light radius of 7.3 kpc, which is very close to that of the stellar component. This corresponds to what is generally found for the molecular distributions (Lisenfeld et al. 2011).

5. Discussion

GRGs are rarer than the RG population, and very few studies have been conducted to detect molecular gas in their host galaxies. We list the detections reported in the literature in Table 4. In the following section, we consider the four GRGs listed in Table 4 that are hosted by early-type galaxies. NGC 315 is the brightest elliptical (cD) galaxy of a group (O'Sullivan et al. 2015), and has also been detected in HI-21cm absorption and emission (Morganti et al. 2009). 3C 31, hosted by NGC 383, is

a lenticular galaxy which is well detected in CO (Evans et al. 2005; Ocaña Flaquer et al. 2010), but neither in emission nor in absorption (Emonts et al. 2010) of HI-21cm. The host of 3C 236 is a massive elliptical galaxy with a distorted morphology, and a prominent dust lane. Its CO spectrum is blue-shifted by $\sim$300 km s^{-1} with respect to the optical velocity (Labiano et al. 2013), and it corresponds to the peak of the HI-21cm absorption (Morganti et al. 2005). The oldest and youngest spectral ages of different parts of GRG 3C 236 are 159 Myr and 51 Myr (Shulevski et al. 2019). The radio core of 3C 326 comprises two early-type galaxies, and the most massive galaxy in the north (3C 326N : 15:52:09.10 +20:05:48.32) is the host galaxy (Rawlings et al. 1990). Its molecular gas in the cold (Nesvadba et al. 2010) and warm phase (Ogle et al. 2007) traces shocks, possibly due to the radio-jet feedback.

Table 4. Properties of GRGs taken from literature.

Name	R_e	SFR	$\log M(H_2)$	$\log M_*$	$\log L_{22\mu m}$	$FWHM$	Refs.
	(kpc)	$(M_\odot \, yr^{-1})$	$(M_\odot)$	$(M_\odot)$	$(erg \, s^{-1})$	$(km \, s^{-1})$	
(1)	(2)	(3)	(4)	(5)	(6)	(7)	(8)
NGC315	6.3	0.63	7.87	11.49	42.18	150	(1)
3C31	4.6	1.02	9.22	11.29	41.51	550	(1)
3C236	7.4	7.51	9.32	11.15	43.07	–	(2)
3C326N	6.9	0.67	9.18	11.40	42.09	351	(3)

Notes. Column 2 lists the half-light radius (R_e), Col. 3 the star formation rate (SFR), Col. 4 the molecular mass ($\log M(H_2)$), Col. 5 the stellar mass ($\log M_*$), Col. 6 the $22\,\mu m$ luminosity derived from WISE ($\log L_{22\mu m}$), and Col. 7 the CO(1-0) line width (FWHM) obtained from the respective references listed in Col. 8.
References. (1) Ocaña Flaquer et al. (2010); (2) Labiano et al. (2013); (3) Nesvadba et al. (2010).
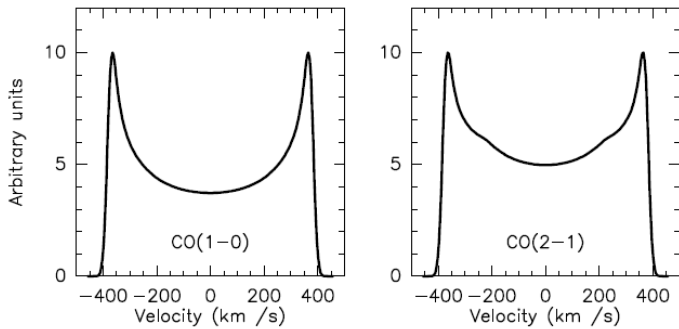

Fig. 6. Spectra obtained from the model for the CO(1-0) line with a beam of $23'' = 33\,kpc$ (*left*) and for the CO(2-1) line with a beam of $12'' = 17\,kpc$ (*right*). The assumed inclination of the disc is $65°$.

5.1. Star formation and gas mass

The host galaxies of GRGs have not previously been studied with respect to their SFR as a function of stellar mass and have not been compared with the main-sequence galaxies, starbursts, or quiescent objects. We show our comparisons in Fig. 7, where the xCOLD GASS sample of Saintonge et al. (2017) is a reference for tracing the main sequence at low redshift and as part of the red sequence. Starburst galaxies at comparable redshifts are plotted from Combes et al. (2011). It is important to have samples at the same z because the location of the main sequence strongly depends on redshift (Whitaker et al. 2012). Eight of our targets are on the main sequence (MS), including the detected R1-1, four are in a starburst phase, and seven are in the red passive sequence. The position close to the MS is associated with disc morphology (Wuyts et al. 2011), and the slope and scatter of the MS depend on morphology (Whitaker et al. 2015).

The star formation rate is expected to be related to the interstellar gas content, and the precise relationship has been discussed either from the atomic or molecular gas or both (Kennicutt 1998; Bigiel et al. 2008). The relation is much tighter and linear with the molecular gas. The relation can be expressed with the global quantities (SFR versus M_{mol}), or with the surface densities, when normalised with the effective area. The latter are computed from the effective radius, containing half of the light (displayed in Table 2). This is a global quantity for the galaxy because we do not resolve the inner parts of the galaxies with our observations with IRAM-30m. However, the relation between the two average surface densities yields another very useful point of view, as discussed by Kennicutt (1998). Figure 8 displays both relations. In the global quantity diagram, most of our upper limits fall in the region of normal MS galaxies, traced by the straight
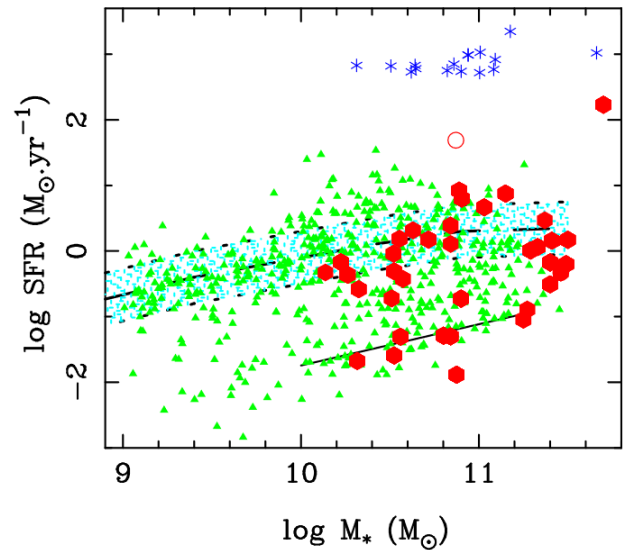

Fig. 7. Location of our targets (red hexagons) in the SFR-M_{star} diagram. They are compared with the xCOLD GASS sample of 532 galaxies with local redshift $0.01 < z < 0.05$ from Saintonge et al. (2017) (green triangles), and with the starburst galaxies (blue stars) in the comparable range $0.2 < z < 0.6$ (Combes et al. 2011). The SDSS main sequence is shown with the cyan-shaded region, and delimited by dashed lines (at ± 0.4 dex), and the red sequence by a full line. Open red circles belong to non-GRGs observed by us.

line corresponding to a depletion time $t_{dep} = M(H_2)/SFR = 1$ Gyr. The R1-1 detected spiral galaxy has a long t_{dep} of 5.5 Gyr, and the tentative detection R2-9 has t_{dep} of 3.15 Gyr, and the two detected GRG (NGC 315 and 3C 236) have an exceptionally short t_{dep} of 120 and 280 Myr, as well as two upper limits that are more typical of starbursts. When normalised to the galaxy surface, the R1-1 spiral galaxy and other outliers fall much closer to the main sequence in the KS diagram, except for NGC 315 and NGC 6251, which are still exceptionally deficient in molecular gas. R1-1, which is a giant spiral galaxy, does not have a high SFR, as seen in Fig. 8, although its reservoir of M_{H2} is large, which may be connected with the restarted nature of the GRG. In these relations, the molecular masses of the starburst sample were obtained with a different CO-to-H_2 conversion factor, as is justified for starbursts (Solomon & Vanden Bout 2005). With a larger factor, the difference to the MS would be much smaller, as is indicated by the arrow in the right panel of Fig. 8.

The fraction of gas in the baryonic content of a galaxy, measured by the ratio of gas to stellar mass, is a key factor in
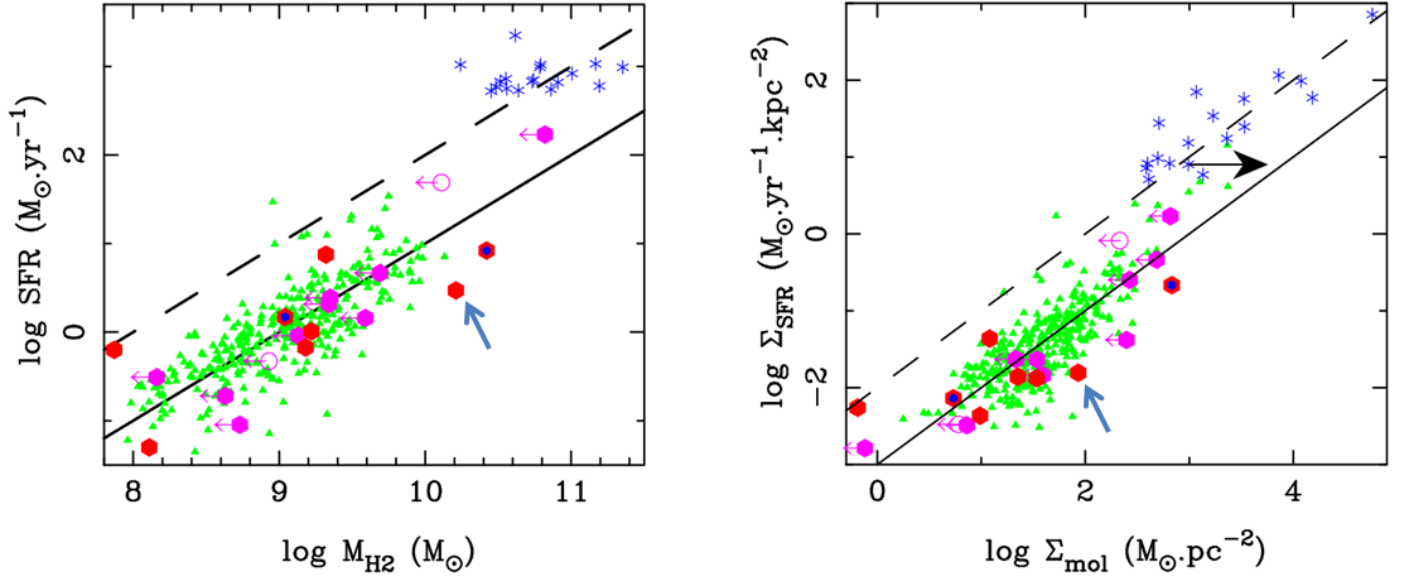
Fig. 8. Star formation rate as a function of the molecular content for our targets compared to normal galaxies and starbursts at comparable redshifts. The global SFR-M_{mol} diagram is shown at the *left*, and the surface densities of the same quantities, representing the unresolved Kennicutt-Schmidt relation (Kennicutt 1998), are shown at the *right*. The straight lines are power laws of slope 1. The full line corresponds to a depletion time of 1 Gyr, and the dashed line to 100 Myr. Symbols are the same as in Fig. 7; upper limits of our targets are shown in pink, and tentative detections as a blue hexagon inside the red one. The blue arrow points to the location of R1-1 (GRG-J2345−0449) in the respective plots.
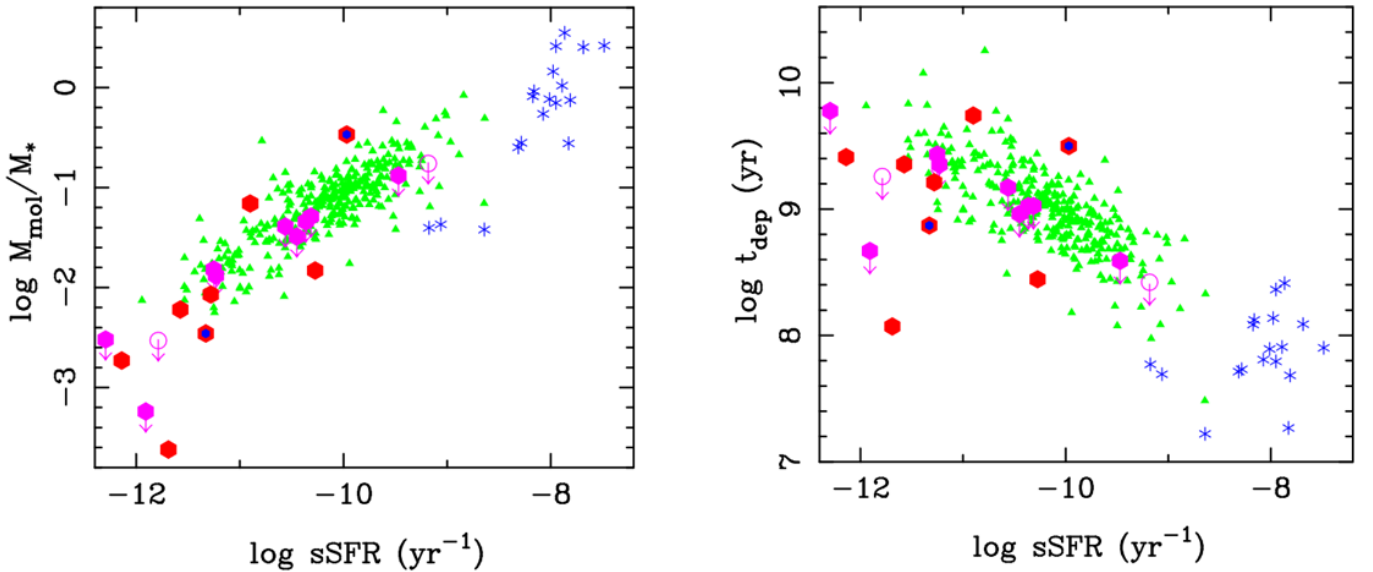

Fig. 9. Trends of specific star formation with other properties: the *left plot* shows the ratio of molecular gas to stellar mass as a function of sSFR. On the *right* we show the depletion time as a function of sSFR. Further details can be found in Sect. 5.1. The symbols in this plot are same as in Fig. 8.

understanding the various observed star formation rates. This relative gas content is plotted versus the specific SFR (sSFR = SFR/M_*) in the left plot in Fig. 9. The GRG targets follow the main-sequence galaxies of the xCOLD GASS sample, two of which are gas-poor, NGC 315 and NGC 6251. Together with the gas fraction, SFR depends on the efficiency of star formation with respect to the amount of fuel, that is, SFR/M_{mol}, which is the inverse of the depletion time t_{dep}. The latter is plotted versus sSFR in the right panel of Fig. 9. Here again, most of our targets follow the MS scaling relations, except for two, NGC 315 and NGC 6251, which appear to be too efficient to form stars because they lack molecular gas. Their t_{dep}

(the inverse of star formation efficiency) is shorter than expected from the scaling relation.

5.2. Radio power and fueling

The nuclear activity in galaxies is thought to be triggered when the central supermassive black hole accretes a significant mass of gas from its interstellar reservoir. Typical accretion phases in AGN may last ~40 million years, with a duty cycle of a few percent (Shankar et al. 2009; Hopkins & Quataert 2010). The GRGs are thought to be at the end of an active and powerful phase of radio galaxy evolution. Several hypotheses have

Table 5. Other properties of GRGs.

Name	FR	log $P_{1.4}$ (W Hz^{-1})	D (Mpc)	HE/LE	Re	Gr/Cl	Q_{Jet} (10^{43} erg s^{-1})
(1)	(2)	(3)	(4)	(5)	(6)	(7)	(8)
R1-1	II	24.31	1.64	LE	Yes	No	–
R1-2	I	23.95	0.96	LE	–	Gr	–
R1-3	II	24.71	1.05	HE	–	Gr	0.53
R2-1	II	25.20	1.52	HE	Yes	–	2.45
R2-2	II	24.57	1.47	HE	–	Gr	–
R2-3	I/II	–	2.48	LE	–	Gr	0.36
R2-4	I/II	24.41	1.96	SF	No	–	1.21
R2-5	II	25.36	2.80	HE	–	Gr	1.77
R2-6	II	25.94	1.79	HE	No	–	17.94
R2-7	II	24.71	2.24	LE		Gr	–
R2-8	II	24.83	1.39	LE	Yes	GR	–
R2-9	II	26.02	1.78	HE	No	–	16.53
NGC 315	I	24.15	1.15	SF	–	Gr	0.16
3C 31	I	24.48	0.93	LE	–	Gr	0.54
3C 236	II	26.05	4.45	HE	Yes	–	14.76
3C 326N	II	25.66	2.02	LE	Yes	–	10.42

Notes. We computed $P_{1.4}$, D, and Q_{Jet} from the data available in the literature, whose details can be found in Sect. 5.2. Column 6 indicates whether the GRG shows signs of restarted AGN activity, and Col. 7 shows their membership in a group (Gr) or cluster (Cl). Sources below the horizontal line are from the literature. The minus indicates non-availability of data or classification.

been proposed to account for their extreme sizes, but the role of each factor is still unclear. The possibilities include the power of the radio jet, implying a higher velocity (Schoenmakers et al. 2000), the effect of the environment (jets are able to extend further in voids, but see Dabhade et al. 2020a), or a restarted activity (Bruni et al. 2019, 2020). In the latter case, the sources are identified with two jets at different orientations, called double-double, or X-shaped (Saripalli et al. 2013), and/or a young central source (Machalski et al. 2007), with a flat spectral index (Schoenmakers et al. 1998), which has recently been refuelled.

The determination of their gas reservoir can confirm and quantify these fueling mechanisms, and help to understand the complex processes involved in their radio-jet launching and evolution. The important clues for the giant nature of GRGs may lie in the accretion rates, which translate into high excitation (HE) or low excitation (LE). The HE objects are defined to have an accretion rate above one-hundredth of the Eddington rate, while the LE objects accrete below this limit. The latter belong to a regime of radiatively inefficient accretion, which foster the formation of radio jets. Table 5 shows our classification of GRGs in our sample with respect to their AGN excitation type, high and low, or HEGRG and LEGRG. We do not find that HEGRGs have higher molecular gas mass than LEGRGs, as was found by Smolčić & Riechers (2011) for RGs. Dabhade et al. (2020a) showed that LEGRGs and HEGRGs have distinct properties, such as their respective small size counterparts LERGs and HERGs. We do not have enough statistics here to see a difference with molecular gas fraction.

Recent gas accretion could be violent, through major mergers, or more secular through minor mergers of cold gas accretion from cosmic filaments. The observation of the molecular component may bring important clues, showing a perturbed component in case of galaxy interaction, or a regular disc for secular evolution. It has been observed that the detection rate of molecular gas is high in the edge-darkened Fanaroff-Riley (FR) type

1 radio galaxy (Fanaroff & Riley 1974) and low in edge brightened FR-II type (Evans et al. 2005). More than 90% of the GRGs have a morphology of FR-II type (Dabhade et al. 2020b,a), and it is very interesting to determine whether GRGs with FR-II type morphology also have fewer molecular gas detections.

Table 5 summarises the FR type, total radio power ($P_{1.4}$), projected linear size (D), excitation state, and jet kinetic power (Q_{Jet}) of all GRGs in our sample along with other GRGs taken from the literature. The 1.4 GHz power was estimated using the NRAO VLA Sky Survey (Condon et al. 1998) flux of the GRG at 1.4 GHz. We used the method described by Hardcastle (2018) to estimate Q_{Jet} using the 150 MHz flux from TIFR GMRT Sky Survey (Intema et al. 2017) and other observations from the literature. A similar scheme was used in Dabhade et al. (2020a) to compute the above parameters for a large sample of GRGs. The excitation state (accretion mode) of GRGs is determined from the mid-infrared fluxes, as in Dabhade et al. (2020a). It helps separate star-forming objects from objects whose emission is dominated by the AGN, as well as HE from LE radio galaxies with the mid-infrared ratios obtained in the WISE bands. WISE colours have been demonstrated to be very useful diagnostics of the accretion mode of radio galaxies (Gürkan et al. 2014).

Evans et al. (2005) conducted a survey to investigate the molecular content in RGs, where they found detections in FR-I and compact sources, but rarely in FR-II objects. It could be expected that restarted RGs, requiring molecular gas to fuel their activity, would be detected, but only a few have been found to be rich in molecular gas, for example, the post-merger 3C293 (Evans et al. 2005; Labiano et al. 2014). Evans et al. (2005) also searched for a possible correlation between the CO luminosity and the 1.4 GHz core luminosity and found none. We studied the possible effect of the radio jets on the host galaxy properties by exploring the connections between Q_{Jet} and parameters derived from our IRAM-30m observations. Based on the current data, we find no correlation between these parameters. These results may not uncover the whole aspect because our observations

with IRAM-30m presents the global cumulative molecular gas properties, and correlations may exist for nuclear region components alone.

GRGs have more intermediate-age stellar populations than the smaller FR-II radio sources (Kuźmicz et al. 2019). This is also true for their neighbours within 1.5 Mpc, which show in general younger populations, suggesting triggered star formation due to their environment. This triggering, either through mergers or cold streams, might also be responsible for their giant sizes. A large fraction of GRGs in our sample belong to groups, like R1-2, R1-3, R2-2, R2-3, R2-5, and R2-7 (cf. Table 5). R2-3, in particular, resides at the centre of a quite disturbed tight galaxy group. It is one of the galaxies of the UGC9555 triplet, hosting a compact flat-spectrum radio source (Clarke et al. 2017). There is evidence that the AGN has been fueled by recent interactions and minor mergers from its group galaxies. None of the other galaxies in the sample shows any signs of recent mergers that might be responsible for their fueling.

Finally, four out of seven of the CO-detected GRGs belong to the restarted class, implying that the molecular gas has recently (within ∼100 Myr) refuelled the AGN and radio jets. However, there seems to be a struggle between star formation and nuclear activity for the fueling. Some of these galaxies are actively forming stars, and their depletion time is quite short (740 Myr and 280 Myr for Speca and 3C236, respectively), while others are rather quiescent and favour the AGN, like R1-1 and 3C326 (with t_{dep} of 5.5 Gyr and 2.26 Gyr). Using observations of the *Hubble* Space Telescope, Tremblay et al. (2010) have shown bursts of repeated star formation in the host galaxy of 3C 236, which has a dusty disc around the AGN. Because 3C 236 is known to be a restarted AGN, this might be connected with the young starburst property of the host galaxy. Based on the studies of GRGs conducted so far and our results, we understand that we observe each GRG in its different evolutionary phase. Therefore we are unlikely to find a similar fueling trend (e.g. cold gas fueling) for all GRGs because the trend closely depends on the AGN accretion state.

In the future, it will be fruitful to observe the GRGs with ALMA to probe the sphere of influence of the black holes that reside in the AGN. This might be a test for the presence of a molecular torus, as was recently found in some low-luminosity AGNs by Combes et al. (2019).

6. Summary

We have presented our first IRAM results for a sample of 12 GRGs, selected from the GRG catalogue (Dabhade et al. 2020a). We detected the two first rotational lines of CO in one GRG, which is the giant spiral GRG-J2345−0449, and report tentative signals for two others (R2-8 and R2-9). The two-horn shape of the spectra of R1-1 (GRG-J2345-0449) allowed us to determine the concentration of the molecular gas in the giant spiral galaxy. The best-fit model is a roughly exponential disc for the molecular component, and its half-light radius is comparable to that of the stellar component.

We added four GRGs from the literature with CO line detections to our sample. Comparing this sample of 16 GRGs with the MS star-forming galaxies at comparable redshift from Saintonge et al. (2017) and a sample of starburst galaxies at similar z (Combes et al. 2011), we find that most (8) of our targets are on the MS, 7 are on the red sequence, and 4 are starbursts. The molecular content of CO-detected GRGs is quite compatible with what is expected from their SFR, although our detected giant spiral appears to be deficient in star formation,

with a depletion time of 5.5 Gyr that is about three times longer than the average of the MS.

Most of the GRGs detected in molecular gas to date are restarted radio galaxies or are in groups, suggesting that the environment plays an important role to refuel the central AGN. The accreted gas also fuels star formation, and the depletion time is sometimes quite short, a few 100 Myr. This is comparable to timescales similar to the spectral ages of the GRGs. Up to now, the number of GRGs with CO detections is low, and more detections are required to draw firmer conclusions.

References

Amirkhanyan, V. R. 2016, Astrophys. Bull., 71, 384
Baars, J. W. M., Hooghoudt, B. G., Mezger, P. G., & de Jonge, M. J. 1987, A&A, 175, 319
Bagchi, J., Vivek, M., Vikram, V., et al. 2014, ApJ, 788, 174
Begelman, M. C., Rees, M. J., & Blandford, R. D. 1979, Nature, 279, 770
Bell, E. F., McIntosh, D. H., Katz, N., & Weinberg, M. D. 2003, ApJS, 149, 289
Bigiel, F., Leroy, A., Walter, F., et al. 2008, AJ, 136, 2846
Bolatto, A. D., Wolfire, M., & Leroy, A. K. 2013, ARA&A, 51, 207
Bregman, J. N., Anderson, M. E., Miller, M. J., et al. 2018, ApJ, 862, 3
Bruni, G., Panessa, F., Bassani, L., et al. 2019, ApJ, 875, 88
Bruni, G., Panessa, F., Bassani, L., et al. 2020, MNRAS, 494, 902
Calzetti, D., Kennicutt, R. C., Engelbracht, C. W., et al. 2007, ApJ, 666, 870
Cantwell, T. M., Bray, J. D., Croston, J. H., et al. 2020, MNRAS, 495, 143
Catalán-Torrecilla, C., Gil de Paz, A., Castillo-Morales, A., et al. 2015, A&A, 584, A87
Chang, Y.-Y., van der Wel, A., da Cunha, E., & Rix, H.-W. 2015, ApJS, 219, 8
Chen, R., Peng, B., Strom, R. G., & Wei, J. 2011, MNRAS, 412, 2433
Chilingarian, I. V., Melchior, A.-L., & Zolotukhin, I. Y. 2010, MNRAS, 405, 1409
Cicone, C., Maiolino, R., Sturm, E., et al. 2014, A&A, 562, A21
Clarke, A. O., Heald, G., Jarrett, T., et al. 2017, A&A, 601, A25
Cluver, M. E., Jarrett, T. H., Hopkins, A. M., et al. 2014, ApJ, 782, 90
Combes, F., García-Burillo, S., Audibert, A., et al. 2019, A&A, 623, A79
Combes, F., García-Burillo, S., Braine, J., et al. 2011, A&A, 528, A124
Condon, J. J., Cotton, W. D., Greisen, E. W., et al. 1998, AJ, 115, 1693
Croton, D. J., Springel, V., White, S. D. M., et al. 2006, MNRAS, 365, 11
Dabhade, P., Gaikwad, M., Bagchi, J., et al. 2017, MNRAS, 469, 2886
Dabhade, P., Mahato, M., Bagchi, J., et al. 2020a, A&A, 642, A153
Dabhade, P., Röttgering, H. J. A., Bagchi, J., et al. 2020b, A&A, 635, A5
De Breuck, C., Neri, R., & Omont, A. 2003, New Astron. Rev., 47, 285
Emonts, B. H. C., Morganti, R., Struve, C., et al. 2010, MNRAS, 406, 987
Emonts, B. H. C., Norris, R. P., Feain, I., et al. 2014, MNRAS, 438, 2898
Evans, A. S., Mazzarella, J. M., Surace, J. A., et al. 2005, ApJS, 159, 197
Fanaroff, B. L., & Riley, J. M. 1974, MNRAS, 167, 31P
Fanti, C., Fanti, R., de Ruiter, H. R., & Parma, P. 1987, A&AS, 69, 57
Gürkan, G., Hardcastle, M. J., & Jarvis, M. J. 2014, MNRAS, 438, 1149
Gürkan, G., Hardcastle, M. J., Jarvis, M. J., et al. 2015, MNRAS, 452, 3776
Hardcastle, M. J. 2018, MNRAS, 475, 2768
Healey, S. E., Romani, R. W., Taylor, G. B., et al. 2007, ApJS, 171, 61
Heckman, T. M., & Best, P. N. 2014, ARA&A, 52, 589
Hernquist, L. 1990, ApJ, 356, 359
Hopkins, P. F., & Quataert, E. 2010, MNRAS, 407, 1529
Hota, A., Sirothia, S. K., Ohyama, Y., et al. 2011, MNRAS, 417, L36
Hughes, D. H., Dunlop, J. S., & Rawlings, S. 1997, MNRAS, 289, 766

Intema, H. T., Jagannathan, P., Mooley, K. P., & Frail, D. A. 2017, A&A, 598, A78

Jennison, R. C., & Das Gupta, M. K. 1953, Nature, 172, 996

Jones, D. L., & Wehrle, A. E. 2002, ApJ, 580, 114

Kennicutt, R. C. Jr. 1998, ARA&A, 36, 189

Kozieł-Wierzbowska, D., & Stasińska, G. 2011, MNRAS, 415, 1013

Kozieł-Wierzbowska, D., Goyal, A., & Żywucka, N. 2020, ApJS, 247, 53

Kuźmicz, A., Jamrozy, M., Bronarska, K., Janda-Boczar, K., & Saikia, D. J. 2018, ApJS, 238, 9

Kuźmicz, A., Czerny, B., & Wildy, C. 2019, A&A, 624, A91

Labiano, A., García-Burillo, S., Combes, F., et al. 2013, A&A, 549, A58

Labiano, A., García-Burillo, S., Combes, F., et al. 2014, A&A, 564, A128

Laing, R. A., Riley, J. M., & Longair, M. S. 1983, MNRAS, 204, 151

Lanz, L., Ogle, P. M., Alatalo, K., & Appleton, P. N. 2016, ApJ, 826, 29

Ledlow, M. J., Owen, F. N., Yun, M. S., & Hill, J. M. 2001, ApJ, 552, 120

Lisenfeld, U., Espada, D., Verdes-Montenegro, L., et al. 2011, A&A, 534, A102

Lynden-Bell, D. 1969, Nature, 223, 690

Machalski, J. 2011, MNRAS, 413, 2429

Machalski, J., & Condon, J. J. 1999, ApJS, 123, 41

Machalski, J., Jamrozy, M., & Zola, S. 2001, A&A, 371, 445

Machalski, J., Koziel-Wierzbowska, D., & Jamrozy, M. 2007, Acta Astron., 57, 227

Magorrian, J., Tremaine, S., Richstone, D., et al. 1998, AJ, 115, 2285

Mao, M. Y., Owen, F., Duffin, R., et al. 2015, MNRAS, 446, 4176

Marconi, A., & Hunt, L. K. 2003, ApJ, 589, L21

Masters, K. L., Mosleh, M., Romer, A. K., et al. 2010, MNRAS, 405, 783

McLure, R. J., Willott, C. J., Jarvis, M. J., et al. 2004, MNRAS, 351, 347

Morganti, R., Tadhunter, C. N., & Oosterloo, T. A. 2005, A&A, 444, L9

Morganti, R., Peck, A. B., Oosterloo, T. A., et al. 2009, A&A, 505, 559

Mukherjee, D., Bicknell, G. V., Sutherland, R., & Wagner, A. 2016, MNRAS, 461, 967

Mukherjee, D., Bicknell, G. V., Wagner, A. e. Y., Sutherland, R. S., & Silk, J. 2018, MNRAS, 479, 5544

Mulcahy, D. D., Mao, M. Y., Mitsuishi, I., et al. 2016, A&A, 595, L8

Nesvadba, N. P. H., Boulanger, F., Salomé, P., et al. 2010, A&A, 521, A65

Nesvadba, N. P. H., Drouart, G., De Breuck, C., et al. 2017, A&A, 600, A121

Nieto, J. L., Coupinot, G., Lelievre, G., & Madsen, C. 1983, MNRAS, 203, 39P

Ocaña Flaquer, B., Leon, S., Combes, F., & Lim, J. 2010, A&A, 518, A9

Ogle, P., Antonucci, R., Appleton, P. N., & Whysong, D. 2007, ApJ, 668, 699

O'Sullivan, E., Combes, F., Hamer, S., et al. 2015, A&A, 573, A111

Owen, F. N., Ledlow, M. J., & Keel, W. C. 1995, AJ, 109, 14

Park, S., Sohn, B. W., & Yi, S. K. 2013, A&A, 560, A80

Prandoni, I., Laing, R. A., de Ruiter, H. R., & Parma, P. 2010, A&A, 523, A38

Proctor, D. D. 2016, ApJS, 224, 18

Rawlings, S., Saunders, R., Miller, P., Jones, M. E., & Eales, S. A. 1990, MNRAS, 246, 21P

Ruffa, I., Prandoni, I., Laing, R. A., et al. 2019, MNRAS, 484, 4239

Saintonge, A., Catinella, B., Tacconi, L. J., et al. 2017, ApJS, 233, 22

Salim, S., Boquien, M., & Lee, J. C. 2018, ApJ, 859, 11

Salomé, Q., Salomé, P., & Combes, F. 2015, A&A, 574, A34

Saripalli, L., & Mack, K. H. 2007, MNRAS, 376, 1385

Saripalli, L., Malarecki, J. M., Subrahmanyan, R., Jones, D. H., & Staveley-Smith, L. 2013, MNRAS, 436, 690

Schoenmakers, A. P., Mack, K. H., Lara, L., et al. 1998, A&A, 336, 455

Schoenmakers, A. P., Mack, K. H., de Bruyn, A. G., et al. 2000, A&AS, 146, 293

Schoenmakers, A. P., de Bruyn, A. G., Röttgering, H. J. A., & van der Laan, H. 2001, A&A, 374, 861

Shankar, F., Weinberg, D. H., & Miralda-Escudé, J. 2009, ApJ, 690, 20

Shulevski, A., Barthel, P. D., Morganti, R., et al. 2019, A&A, 628, A69

Singh, V., Ishwara-Chandra, C. H., Sievers, J., et al. 2015, MNRAS, 454, 1556

Smolčić, V., & Riechers, D. A. 2011, ApJ, 730, 64

Solomon, P. M., & Vanden Bout, P. A. 2005, ARA&A, 43, 677

Tacconi, L. J., Genzel, R., Saintonge, A., et al. 2018, ApJ, 853, 179

Taylor, G. L., Dunlop, J. S., Hughes, D. H., & Robson, E. I. 1996, MNRAS, 283, 930

Toomre, A. 1964, ApJ, 139, 1217

Tremblay, G. R., O'Dea, C. P., Baum, S. A., et al. 2010, ApJ, 715, 172

van den Bosch, R. C. E., Gebhardt, K., Gültekin, K., et al. 2012, Nature, 491, 729

van Ojik, R., Roettgering, H. J. A., van der Werf, P. P., et al. 1997, A&A, 321, 389

Véron-Cetty, M. P., & Véron, P. 2006, A&A, 455, 773

Waggett, P. C., Warner, P. J., & Baldwin, J. E. 1977, MNRAS, 181, 465

Walker, S. A., Bagchi, J., & Fabian, A. C. 2015, MNRAS, 449, 3527

Whitaker, K. E., van Dokkum, P. G., Brammer, G., & Franx, M. 2012, ApJ, 754, L29

Whitaker, K. E., Franx, M., Bezanson, R., et al. 2015, ApJ, 811, L12

Wiklind, T., Combes, F., Henkel, C., & Wyrowski, F. 1997, A&A, 323, 727

Willis, A. G., Strom, R. G., & Wilson, A. S. 1974, Nature, 250, 625

Winter, L. M., Mushotzky, R. F., Tueller, J., & Markwardt, C. 2008, ApJ, 674, 686

Wright, E. L., Eisenhardt, P. R. M., Mainzer, A. K., et al. 2010, AJ, 140, 1868

Wuyts, S., Förster Schreiber, N. M., van der Wel, A., et al. 2011, ApJ, 742, 96

Young, L. M., Bureau, M., Davis, T. A., et al. 2011, MNRAS, 414, 940